Nanoscale

PAPER

View Article Online
View Journal | View Issue

Cite this: *Nanoscale*, 2022, **14**, 1333

Complex supramolecular tessellations with on-surface self-synthesized C_{60} tiles through van der Waals interaction†

Xin Zhang,[a] Haoxuan Ding,[b] Xiaorui Chen,[c] Haiping Lin,[c] Qing Li,[c] Jianzhi Gao,*[c] Minghu Pan*[c] and Quanmin Guo*[b]

Received 25th August 2021,
Accepted 11th December 2021

DOI: 10.1039/d1nr05589e

rsc.li/nanoscale

Supramolecular tessellation with self-synthesized $(C_{60})_7$ tiles is achieved based on a cooperative interaction between co-adsorbed C_{60} and octanethiol (OT) molecules. Tile synthesis and tiling take place simultaneously on a gold substrate leading to a two-dimensional lattice of $(C_{60})_7$ tiles with OT as the binder molecule filling the gaps between the tiles. This supramolecular tessellation is featured with simultaneous on-site synthesis of tiles and self-organized tiling. In the absence of specific functional groups, the key to ordered tiling for the C_{60}/OT system is the collective van der Waals (vdW) interaction among a large number of molecules. This bicomponent system herein offers a way for the artificial synthesis of 2D complex vdW supramolecular tessellations.

Introduction

Two-dimensional (2D) supramolecular structures have been studied for many years due to their rich structural configurations,[1] flexible fabrication methods[2] and a wide range of applications in nanotechnology.[3–6] One attractive approach for the fabrication of 2D molecular materials is tiling a solid surface with molecules of specific geometric shapes.[7,8] As far as the tessellation composition is concerned, two types of molecular tiles have been reported over the past few decades. One is the system composed of a single component in which molecules with linear,[9] triangular,[10] rhombic[11] or other regular and semi-regular shapes and configurations[12] serve as building blocks and linkers to achieve polygonal tessellation. By comparison, multicomponent systems are more versatile for creating more complex supramolecular tessellations.[1,13–16] Effects of spatial confinement and molecular crowding between different kinds of components can prevent molecules, especially the molecules without specific functional groups, from forming a close-packed arrangement[17,18] and hence facilitate the formation of various supramolecular structures. Meanwhile, the aggregation of various numbers of molecules into clusters can be exploited as a means of on-surface synthesis of new tiles.[19] In particular, the preferential formation of magic number clusters offers high selectivities towards the creation of certain types of tiles.[20]

The balance between intermolecular interaction and the molecule–substrate interaction determines the architecture as well as the properties of supramolecular tessellations. Relatively weak interactions give flexibility in the tiling patterns with pure van der Waals interaction being the extreme case. The challenge in van der Waals tiling is to maintain stable intermolecular interactions against thermal disturbance. Although the use of vdW force is limited due to the lack of specific and directional bonding, it has been proved to be effective in nonplanar and extended molecular assembly.[21,22] For example, the magic number $(C_{60})_7$–$(Au)_{19}$ hybrid cluster has been prepared based on the unique property of the vdW force in our previous work.[23] Here, we explore a bicomponent system consisting of octanethiol (OT) and C_{60} molecules. We aim to fabricate C_{60} cluster tiles with a specific number of molecules and further bind the supramolecular tiles together. We report on the on-surface self-synthesis of $(C_{60})_7$ tiles and the tiling of Au(111) with such tiles utilizing OT as the "grout". We also discuss a related tessellation where chains of C_{60} act as rectangular tiles. Controlling the assembly of C_{60} molecules with pre-adsorbed or co-adsorbed molecules has been extensively studied[24] and many examples have been discussed in a recent review article.[25]

Results and discussion

$(C_{60})_7$ based supramolecular tiling

When two types of molecules are co-adsorbed on a solid surface, their relative concentration is usually an important

[a]School of Physics, Northwest University, 710069, China
[b]School of Physics and Astronomy, University of Birmingham, Birmingham B15 2TT, UK. E-mail: Q.GUO@bham.ac.uk
[c]School of Physics and Information Technology, Shaanxi Normal University, Xi'an 710119, China. E-mail: jianzhigao@snnu.edu.cn, minghupan@snnu.edu.cn

†Electronic supplementary information (ESI) available. See DOI: 10.1039/d1nr05589e

control parameter. In a previous study, we observed the formation of porous C_{60} frameworks with OT filling the pores.[17] The C_{60}/OT ratio can be changed by heating the sample up. The desorption temperature of OT is more than 200 K lower than that for C_{60}, hence the coverage of OT can be reduced by gentle heating of the sample with little effect on the coverage of C_{60}. As the C_{60}/OT ratio increases, we observe a gradual transition from porous C_{60} network to C_{60} tiles. Fig. 1(a) shows an STM image of a mixed C_{60}/OT layer. In this image, one can see three distinct structures: (i) a porous C_{60}/OT framework[17] which occupies about 80% of the surface; (ii) a pure striped phase of OT exhibiting parallel rows; and (iii) patches of $(C_{60})_7$ tiles which are shaded with light purple colour. A magnified view of the $(C_{60})_7$ tiles alongside the porous framework is shown in Fig. 1(b). Each tile consists of seven C_{60} molecules. The molecules within the $(C_{60})_7$ tile are close-packed giving rise to a perfect hexagonal shape. The molecule in the centre of the tile has a lower apparent height and appears darker in the false colour image. The other six molecules appear the same in the image. The phenomenon of brightness contrast in C_{60}/Au(111) has been reported before.[26–29] One of the reasons for the observed contrast is different molecular orientations. There is a clear gap between two adjacent $(C_{60})_7$ tiles. We cannot resolve the detailed structure within the gap, but the gap must be filled by molecules which have to be OT in this case. A vacant gap between two $(C_{60})_7$ clusters is not stable at RT. The OT rows in the striped phase are known to align in the $[11\bar{2}]$ direction.[17] Using the OT row as a reference, the azimuthal orientation of the $(C_{60})_7$ clusters can be determined. As shown in Fig. 1(b), the row of the $(C_{60})_7$ tiles is oriented at ±14 degrees from the $\langle 1\bar{1}0\rangle$ direction of Au(111). This azimuthal orientation has been reported in a 7 × 7 R14° superstructure in which C_{60} molecules are closely packed on Au(111).[26]

The formation of the C_{60} heptamer unit has been reported on several occasions.[28] There is a tendency for the central C_{60} molecule to occupy a stable site allowing efficient charge transfer from the Au substrate into this molecule. It was reported that the central C_{60} molecule is bonded to the substrate *via* one of the faces of the hexagon. We imaged the $(C_{60})_7$ tile under both positive and negative sample bias voltages as shown in Fig. 2. The C_{60} molecule in the centre of the tile shows clear bias polarity dependent contrast. As can be seen in Fig. 2(b), the central C_{60} molecular appears brighter under negative bias and dimmer under positive bias. This bias polarity dependence suggests an electronic effect contributing to the observed height differences. Based on what has been reported previously, we speculate that the central C_{60} molecule sits on the substrate with its hexagonal face touching Au. Electron transfer from Au(111) into the empty orbitals of the central C_{60} makes it electron rich. We do not know the orientations of the other six molecules within the tile. At room temperature, it is likely that the other six molecules do not have a fixed orientation and they keep flipping under thermal agitation. Thus, the STM image may show time averaged features of the other six molecules. In this study, we have not performed imaging at low temperatures and hence the orientation of the C_{60} molecules is not accurately determined. The central C_{60} molecule appears to be stable at RT although flipping can be observed occasionally. In Fig. 2(a), the tile highlighted by a green circle shows the central molecule bright under positive sample bias. This indicates that the central molecule in this tile has flipped under the influence of the STM tip. In Fig. 2(c), the same molecule resumes its normal dim state.

The above discussion for the different molecular adsorption characteristics in $(C_{60})_7$ cluster leads to an understanding that the central molecule in the $(C_{60})_7$ cluster can serve as an "anchor" fixed on the gold surface, and the other six molecules are expected to be less strongly bound to the Au(111) substrate. van der Waals force among all seven molecules contributes to the stability of the tile. However, the intermolecular force among the C_{60} molecules alone is not sufficient to protect the integrity of the tile as such heptamer tiles do not form with only C_{60} on the Au(111) surface. Pure heptamers of C_{60} are not stable on Au(111) at RT. However, they can be stabilized using metal coordination[23] or by confinement in molecular cavities.[30] The formation of the heptamer tiles observed in this work is assisted by the presence of the OT molecules. In the following, we will present structural models for OT assisted tiling.

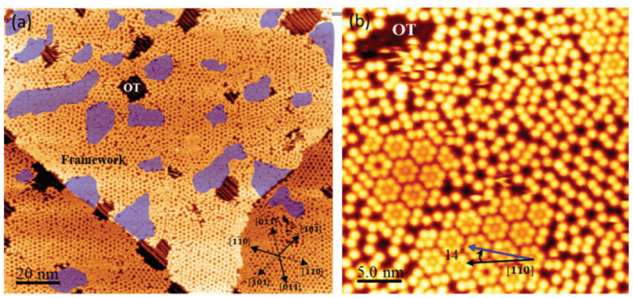

Fig. 1 (a) Large-scale STM image showing the coexistence of (i) porous C_{60}/OT framework; (ii) striped phase of pure OT; and (iii) $(C_{60})_7$ based supramolecular tessellations. (V = 2 V, I = 50 pA) (b) magnified view of a region with the tiled area sitting next to the porous framework. The $(C_{60})_7$ tiles are aligned in a direction that is rotated by 14 degrees clockwise from the $[1\bar{1}0]$ direction. (V = 1.5 V, I = 50 pA).

Model of $(C_{60})_7$–OT_6 bicomponent tiling

Having investigated the morphology and electronic properties of the individual $(C_{60})_7$ cluster, we now focus on the tiling mechanism. Fig. 3(a) reveals the detailed structure of the bicomponent tiling. The high-resolution STM image shows a periodic molecular arrangement with six-fold symmetry, which is supported by the corresponding fast Fourier transform (FFT) pattern in the inset. The unit cell of the supramolecular tessellation highlighted by the blue rhombus has a hexagonal lattice (c = 3.16 ± 0.01 nm, α = 60°). These well-defined lattice constants help us to establish the optimal model of $(C_{60})_7$ based supramolecular tessellation. The lattice constant measured by STM is subject to uncertainties due to thermal drift and the creep of the piezo scanner. However, the lattice structure

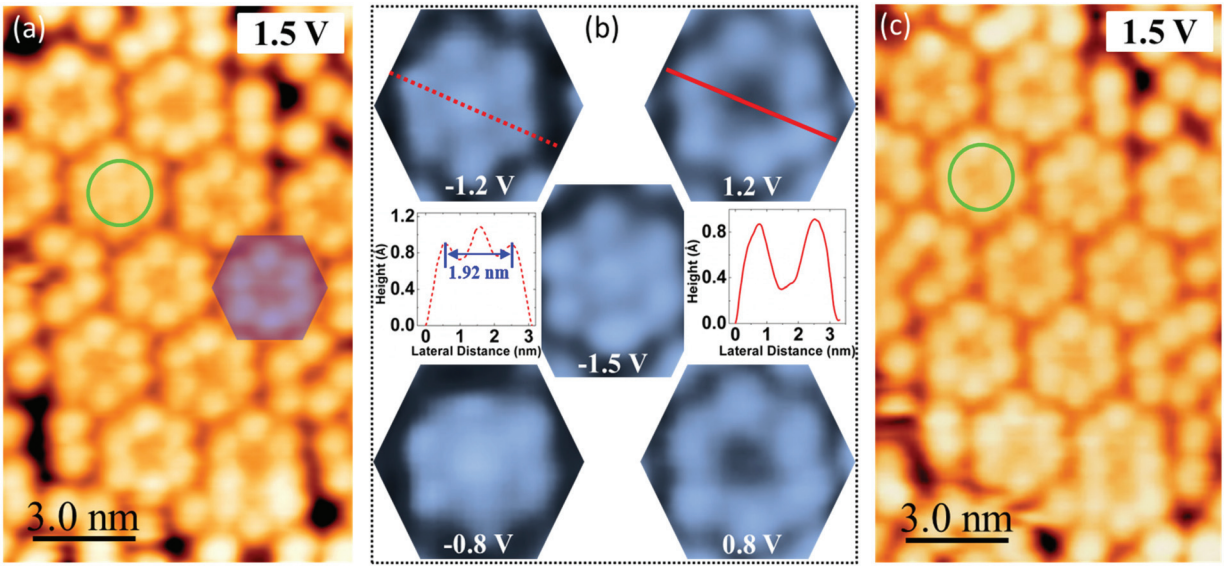

Fig. 2 Bias-dependent characteristics of the tile. (a) and (c) are images from the same area of the sample acquired with +1.5 V sample bias. The green circles highlight the flipping of the central C_{60} molecule under imaging conditions. (b) STM observation of bias dependence of the $(C_{60})_7$ cluster shaded with the light blue hexagon in (a). Images are acquired under the same tunnel current of 50 pA with the bias voltage set at ±0.8 V and ±1.2 V. The line profiles in the inset are along the lines in the upper images.

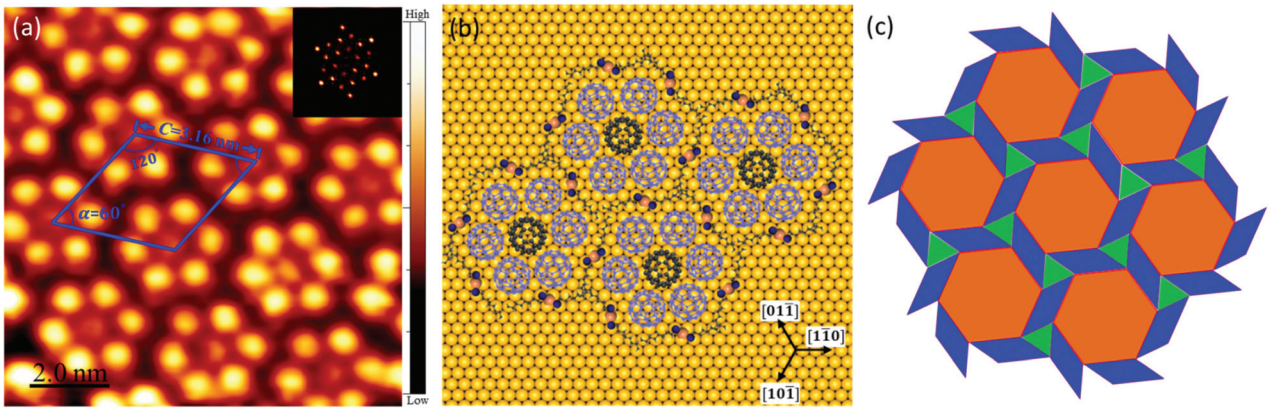

Fig. 3 (a) High-resolution STM image of the $(C_{60})_7$ based supramolecular structure. The inset shows the corresponding FFT pattern. (V = 0.5 V, I = 100 pA) (b) optimized ball model of the unit cell in (a). The blue and black C_{60} cages correspond to the central and surrounding C_{60} molecules respectively. The RS–Au–SR staples are arranged around the $(C_{60})_7$. (c) Schematic block diagram of the $(C_{60})_7$ based supramolecular tessellation.

requires that at least the dim C_{60} molecule occupy an identical site on Au(111). Our analysis leads to the structural model shown in Fig. 3(b). According to the model in Fig. 3(b), the distance between the two adjacent tiles is $\sqrt{117}a$ (a = 2.889 Å), which is very close to our experimental measurement of 3.16 nm. The lattice of the tiles is thus defined as $\left(\sqrt{117}a \times \sqrt{117}a\right)R14°$. The patches of close-packed C_{60} can be used as a reference to determine the adsorption site for C_{60} molecules in the tile. The adsorption site for C_{60} molecules inside the extended domains of close-packed C_{60} is the site on the top.[28] Using this as a reference, we find that the central C_{60} in the tile occupies a hollow site (see Fig. S1 in the ESI†). The six surrounding molecules do not occupy the same type of hollow site. They are all shifted slightly towards the central molecule. It seems that in order to optimize the C_{60}–C_{60} distance, the surrounding C_{60} molecules take a less favourable adsorption site in terms of the C_{60}–Au(111) interaction. Fig. 3(b) shows the best structural model derived from our analysis. According to this model, the distance between the central molecule and each of the six surrounding molecules is 0.96 ± 0.01 nm which is slightly shorter than the typical nearest neighbour distance, 1 nm,[31,32] within either C_{60} crystals or in the closed-packed layer of C_{60} on Au (111).

We use the close-packed C_{60} domain as the calibration standard and we take 1 nm as the nearest neighbour distance for close-packed C_{60}. The shorter distance measured between the central molecule and the surrounding molecules within the C_{60} heptamer is not due to uncertainty in the experiment. The reason for the observed short distance is due to the coordination number. As we have discussed already, C_{60} molecules on Au(111) have the tendency to form heptamers.[26] An extended 2D close-packed layer of C_{60} sometimes contains an ordered array of C_{60} heptamers as shown by STM images acquired at cryogenic temperatures.[28] At room temperature, the heptamers lose their characteristics due to random thermal flipping of the molecules. For the C_{60} tiles reported here, there is a gap between neighbouring tiles with the gap filled by OT molecules. The molecule in the centre of the tile has six nearest neighbours. Each of the surrounding six molecules has a much lower coordination number of three. This undercoordination may lead to a relaxation of the C_{60}–C_{60} distance, similar to what happens on a solid surface where the distance between the first two layers of atoms is reduced.

Since the molecule in the centre of the tile appears more stable, it gives rise to an apparent anchoring effect where six molecules nest around an "anchoring" molecule. However, the stability of the heptamer arises from the collective interaction of all seven molecules. Bias dependent imaging shows clear charge transfer from Au(111) to the central C_{60} molecule making it electron rich. Occasional flipping of the central molecule has been observed although such thermal flipping seems to be assisted by the scanning tip. The collective vdW interaction among OT and C_{60} molecules is employed to stabilize the fabricated supramolecular tessellation. We finally add the RS–Au–SR ($R{=}CH_3(CH_2)_7S$) alkanethiol staples, which is the basic structure of OT assembly on Au(111), into the space between neighbouring $(C_{60})_7$ clusters. Following the well documented rule that gold adatom in the staple must occupy the bridge site and the axis of staple perpendicular to the bridge,[33] we determine the adsorbed location of OT molecules. Fig. 3(b) shows the optimal unit cell model, in which OT molecules periodically arranged around the $(C_{60})_7$ clusters. Such a unit cell is composed of seven C_{60} and six OT molecules with a low molecular coverage of 0.058 ML and 0.05 ML respectively. The composition of $(C_{60})_7$ based supramolecular tessellation is hence $(C_{60})_7$–$(OT)_6$.

Fig. 3(c) gives the coloured tessellation of a partial 2D periodic tile pattern. The yellow and blue tiles correspond to $(C_{60})_7$ clusters and RS–Au–SR staples respectively. Each $(C_{60})_7$ cluster is separated with a uniform spatial interval by RS–Au–SR alkanethiol staples to form a periodic structure. These equivalent RS–Au–SR staples, as a tiling "binder", span the overall plane to hold C_{60} clusters together by the operation of 60° rotations in this 2D supramolecular tessellation. Because of the relatively high coverage of OT molecules before C_{60} adsorption, the flexible alkyl chains in the regular tessellation are not necessarily parallel to the substrate strictly at ambient temperature. The green triangular tiles represent the region enclosed by the end groups of each of three alkyl chains. Thus the 2D tessellation without overlaps and gaps in Fig. 3(c) can be used to describe the $(C_{60})_7$ based supramolecular structures based on the collective vdW interaction among molecules.

Tessellation evolution induced by thermal treatment

From the $(C_{60})_7$ based supramolecular tessellation discussed above, the dim molecule with a hexagon fixed to Au(111) is vital for the supramolecular structural construction. According to previous studies, thermal annealing is an effective way for tuning molecular adsorption configurations and assembly.[34–38]

Thus, it is expected that more supramolecular tessellations can be fabricated through thermal treatment.

As the sample is heated to higher temperatures, OT coverage is preferentially reduced due to its much lower desorption temperature than that for C_{60}. Following thermal annealing at 120 degrees for 90 minutes, we observed a new tiling structure composed of C_{60} nanochains as shown in Fig. 4(a). There is also simultaneous formation of close-packed C_{60} domains. Interestingly, all of the segments in the C_{60} chains are staggered and rotated 14 degrees clockwise or counter-clockwise with respect to $\langle 1\bar{1}0\rangle$ directions of Au(111), which is consistent with the growth direction of the $(C_{60})_7$ based supramolecular tessellation. The histogram in Fig. 4(b) shows the distribution of the C_{60} molecular number in different $(C_{60})_n$–$(OT)_m$ segments. Molecular rows consisting of three, four or five molecules are the most abundant. The magnified STM image in Fig. 4(c) reveals the detailed configurations of the regular nanochain tessellation. After thermal treatment, the symmetry of the supramolecular structure is reduced to two-fold symmetry (see the FFT pattern in the inset of Fig. 4(c)). The unit cell is labelled by a blue quadrilateral. In the long-chain direction there is no spacing between adjacent molecules. However, in the $[1\bar{1}0]$ direction segments in bright and dim features are arranged periodically with a period of 2.62 ± 0.01 nm. This distance is excellently consistent with $9a$. The apparent height difference (0.39 Å) between bright and dim segments is identical to the observation of $(C_{60})_7$ clusters under the same sample bias, which is proved essentially due to the different submolecular orientations.[27] Compared with the $(C_{60})_7$ based supramolecular tessellation, the number of C_{60} molecules with dim appearance is significantly increased. Half of the C_{60} molecules, broadly speaking, appear with the dim feature in the C_{60} nanochain tessellation.

In analogy with the modelling approach mentioned above, we fill RS–Au–SR staples into the space between bright and dim chains. Fig. 4(e) shows the proposed model of segments with $(C_{60})_3$–OT_2 composition. This assembly model leaves RS–Au–SR staples almost parallel to the Au(111) surface with larger tilting angles of alkyl chains. The length of individual RS–Au–SR staple in the proposed configuration is about 2.23 nm. This length is essential for interpreting the statistical results of the histogram in Fig. 4(b). First, the distance of 2.23 nm is larger than that of the segments composed of two C_{60} molecules. Therefore, C_{60} molecules prefer to grow along the long-chain direction rather than change molecular align-

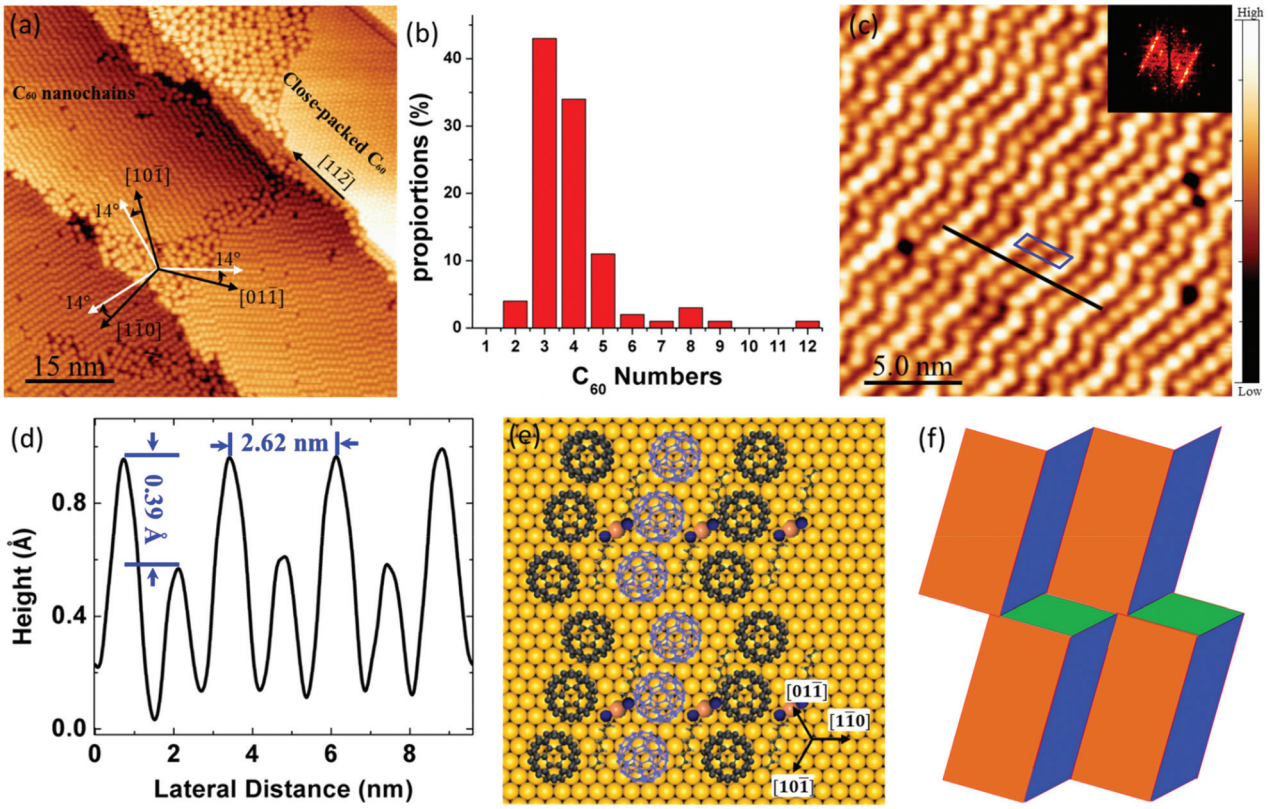

Fig. 4 (a) STM image of the nanochains coexisting with frameworks and close-packed C_{60} domains. (V = 1.8 V, I = 300 pA) (b) the histogram shows the proportion of C_{60} numbers in different short segment of nanochains. (c) Magnified view of nanochains with the corresponding FFT pattern in the inset. (V = 1.5 V, I = 100 pA) (d) line profile along the black straight line in (b). (e) The structure diagram for C_{60}–OT nanochains, in which the blue and dark C_{60} balls represent the bright and dim C_{60} molecules in (c). (f) Scheme of $(C_{60})_n$–OT_m nanochain tessellation.

ment by bending the alkyl chains in the RS–Au–SR staples. Considering the range of the vdW interaction, the segment composed of three C_{60} molecules is the ideal alignment. Second, the tilting angle of alkyl chains should be small in order to fully fill into the space between the neighbouring segments consisting of two C_{60} molecules while the lower coverage of thiol after thermal annealing readily leads to larger tilting angles.[39] Thus few segments containing two C_{60} molecules are observed in our experiment.

Our present work shows that a large number of six-membered segments should cover the substrate surface considering the ideal three-membered segment tiling. However, the proportion of six-membered segments is smaller than four-membered and five-membered segments. This is because the displacement of OT around the C_{60} molecules after thermal annealing is random, thus the relative position of neighbouring RS–Au–SR staples is hard to be determined exactly. We can only speculate at the moment that a small interval between neighbouring RS–Au–SR staples leads to the segment consisting of four or five C_{60} molecules, while a relatively large space results in the formation of two staggered three-membered segments instead of one six-membered segment. Furthermore, the C_{60} chains with longer segment arrangement need more RS–Au–SR staples aligned closely to bind the neighbouring C_{60} chains. This is not possible for OT molecules with low coverage after thermal annealing. The extra space is introduced at each segment junction, which facilitates the formation of large area nanochains. Fig. 4(f) shows the scheme of $(C_{60})_3$–$(OT)_2$ nanochains corresponding to the optimal tiling model in Fig. 4(e). The yellow, blue and green quadrilaterals represent C_{60} segments, alkanethiol staples and the interval space respectively. The results enlighten us to tune the supramolecular tessellation configurations by changing the alkyl chain length of thiol molecule.

Conclusions

In summary, we succeeded in fabricating C_{60} based 2D supramolecular tessellations on Au(111) surface based mainly on a cooperative van der Waals interaction. No functional groups are required for specific bonding between the neighbouring tiles for this system. The $(C_{60})_n$ tiles are self-synthesized on site and the space between the tiles are filled by the binder molecule OT. This work clearly demonstrates the vital role of vdW interaction in complex 2D supramolecular tessellations. In par-

ticular, the anchored molecule in the centre of a $(C_{60})_7$ cluster enhances the stability of supramolecular tessellations. Our work may represent a case study for C_{60} molecular orbital tuning considering the regular variation of C_{60} molecular adsorption configuration after thermal treatment. The C_{60}–OT supramolecular tiles we introduced here have a number of implications for fabrication and regulation of complex bicomponent supramolecular tessellations. The involvement of the vdW interaction opens more pathways for less strongly bound but more versatile molecular tessellations.

Methods

Experiments were performed at room temperature (RT) using an Omicron variable temperature scanning tunnelling microscope (VT-STM) in ultrahigh vacuum at a base pressure in the order of 10^{-10} mbar. The Au(111) substrate is a 300 nm thick film prepared by depositing gold atom onto a graphite substrate in an ultrahigh vacuum chamber. Many cycles of Ar^+ sputtering and annealing in ultrahigh vacuum were performed for surface cleaning. The energy of the Ar^+ ions is 1 keV. Sputtering at RT generated vacancy defects which disappeared following annealing at above 700 K. The surface prepared as such was clean and almost free from defects. The STM was calibrated using the single atomic layer Au steps and the dimensions of the herringbone reconstructed surface unit cell. Self-assembled monolayer of OT was formed on Au(111) by immersing the sample in 1 mM octanethiol/ethanol solution for 24 h. The sample was then introduced into the vacuum system where it was thermally annealed at 393 K for 3 h. This annealing process caused partial desorption of the OT and the formation of a striped phase.[17] C_{60} molecules were deposited onto the sample with the striped phase of OT at RT. Mixing of C_{60} and OT through molecular diffusion gave rise to a range of bicomponent structures including C_{60} tiles. STM images were collected using electrochemically polished tungsten tips. The full coverage phase of OT on Au(111) was not used because C_{60} was unable to mix with the pre-adsorbed OT molecules. The lateral distance measured was given an uncertainty of ±0.01 nm. This does not mean that features separated by 0.01 nm could readily be determined from a single measurement. Due to the nature of the periodic structure being measured, a distance spanning many unit cell dimensions was measured. Based on many such measurement, we were able to obtain lateral distance values with an ultimate accuracy of ±0.01 nm. Such a degree of accuracy is not necessary though in the process of determining the structure of C_{60} tiles. The long-range order of the tiles, together with the measured values, was used in establishing the adsorption sites of individual C_{60} molecules.

Conflicts of interest

There are no conflicts to declare.

Acknowledgements

This work was financially supported by the National Natural Science Foundation of China (Project Codes 91745115 and 21972083), the China Postdoctoral Science Foundation (2021M692615), the Natural Science Basic Research Program of Shaanxi (no. 2021JQ-297) and Fundamental Research Funds for the Central Universities (GK201901005).

References

1 G. Li, Y. Y. Zhang, H. Guo, L. Huang, H. L. Lu, X. Lin, Y. L. Wang, S. X. Du and H. J. Gao, *Chem. Soc. Rev.*, 2018, **47**, 6073–6100.
2 G. Dominic, E. Maryam, R. Federico, A. Arramel, F. Yuan, D. F. Steven, T. Steven, W. Chen, B. Peter, W. Andrew, P. S. Weiss and D. F. Perepichka, *ACS Nano*, 2018, **12**, 7445–7481.
3 Z. W. Wang, J. J. Qiu, X. S. Wang, Z. P. Zhang, Y. H. Chen, X. Huang and W. Huang, *Chem. Soc. Rev.*, 2018, **47**, 6128–6174.
4 G. Liu, C. Zhen, Y. Y. Kang, L. Z. Wang and H. M. Cheng, *Chem. Soc. Rev.*, 2018, **47**, 6410–6444.
5 Y. Liu, X. D. Duan, Y. Huang and X. F. Duan, *Chem. Soc. Rev.*, 2018, **47**, 6388–6409.
6 F. Wang, Z. X. Wang, L. Yin, R. Q. Cheng, J. J. Wang, Y. Wen, T. A. Shifa, F. M. Wang, Y. Zhang, X. Y. Zhan and J. He, *Chem. Soc. Rev.*, 2018, **47**, 6296–6341.
7 F. Cheng, X. J. Wu, Z. X. Hu, X. F. Lu, Z. J. Ding, Y. Shao, H. Xu, W. Ji, J. S. Wu and K. P. Loh, *Nat. Commun.*, 2018, **9**, 4871.
8 M. Z. Liu, X. L. Zheng, V. Grebe, M. X. He, D. J. Pine and M. Weck, *Angew. Chem., Int. Ed.*, 2021, **60**, 5744–5748.
9 C. Jing, B. D. Zhang, S. Synkule, M. Ebrahimi, A. Riss, W. Auwarter, L. Jiang, G. Medard, J. Reichert, J. V. Barth and A. C. Papageorgiou, *Angew. Chem., Int. Ed.*, 2019, **58**, 18948–18956.
10 Y. T. Shen, K. Deng, S. L. Yang, B. Qin, S. Y. Cheng, N. B. Zhu, J. J. Ding, D. H. Zhao, J. Liu, Q. D. Zeng and C. Wang, *Nanoscale*, 2014, **6**, 7221–7225.
11 M. O. Blunt, J. C. Russell, M. D. Gimenez-Lopez, J. P. Garrahan, X. Lin, M. Schroder, N. R. Champness and P. H. Beton, *Science*, 2008, **322**, 1077–1081.
12 J. A. Millan, D. Ortiz, G. van Anders and S. C. Glotzer, *ACS Nano*, 2014, **8**, 2918–2928.
13 D. L. Cui, M. Ebrahimi, J. M. Macleod and F. Rosei, *Nano Lett.*, 2018, **18**, 7570–7575.
14 T. Wang, Q. T. Fan, L. Feng, Z. J. Tao, J. M. Huang, H. X. Ju, Q. Xu, S. W. Hu and J. F. Zhu, *ChemPhysChem*, 2017, **18**, 3329–3333.
15 Z. G. Song, X. T. Sun and L. W. Wang, *J. Phys. Chem. Lett.*, 2020, **11**, 9224–9229.
16 R. Wang, C. Z. He, W. X. Chen, C. X. Zhao and J. R. Hou, *Chin. Chem. Lett.*, DOI: 10.1016/j.cclet.2021.05.024.
17 X. Zhang, X. Fan, G. Q. Zhu, Y. T. Wang, H. X. Ding, H. P. Lin, Y. Y. Li, Q. Li, J. Z. Gao, M. H. Pan and Q. M. Guo, *J. Phys. Chem. C*, 2020, **124**, 12589–12595.

18 Q. T. Fan, J. M. Gottfried and J. F. Zhu, *Acc. Chem. Res.*, 2015, **48**, 2484–2494.
19 X. Bouju, C. Mattioli, G. Franc, A. Pujol and A. Gourdon, *Chem. Rev.*, 2017, **117**, 1407–1444.
20 A. Pinkard, A. M. Champsaur and X. Roy, *Acc. Chem. Res.*, 2018, **51**, 919–929.
21 J. MacLeod, *J. Phys. D: Appl. Phys.*, 2020, **53**, 043002.
22 Y. Q. Zhang, M. Paszkiewicz, P. Du, L. D. Zhang, T. Lin, Z. Chen, S. Klyatskaya, M. Ruben, A. P. Seitsonen, J. V. Barth and F. Klappenberger, *Nat. Chem.*, 2018, **10**, 296–304.
23 Y. C. Xie, L. Tang and Q. Guo, *Phys. Rev. Lett.*, 2013, **111**, 186101.
24 M. Di Marino, F. Sedona, M. Sambi, T. Carofiglio, E. Lubian, M. Casarin and E. Tondello, *Langmuir*, 2010, **26**, 2466–2472.
25 Y.-F. Geng, Q.-D. Zeng and C. Wang, *Nano Res.*, 2019, **12**, 1509–1537.
26 G. Schull and R. Berndt, *Phys. Rev. Lett.*, 2007, **99**, 226105.
27 J. A. Gardener, G. A. D. Briggs and M. R. Castell, *Phys. Rev. B: Condens. Matter Mater. Phys.*, 2009, **80**, 235434.
28 L. Tang, Y. C. Xie and Q. Guo, *J. Chem. Phys.*, 2011, **135**, 114702.
29 H. Shin, A. Schwarze, R. D. Diehl, K. Pussi, A. Colombier, E. Gaudry, J. Ledieu, G. M. McGuirk, L. N. S. Loli and V. Fournee, *Phys. Rev. B: Condens. Matter Mater. Phys.*, 2014, **89**, 245428.
30 J. A. Theobald, N. S. Oxtoby, M. A. Phillips, N. R. Champness and P. H. Beton, *Nature*, 2003, **424**, 1029–1031.
31 R. J. Wilson, G. Meijer, D. S. Bethune, R. D. Johnson and D. D. Chambliss, *Nature*, 1990, **348**, 621–622.
32 J. L. Wragg, J. E. Chamberlain, H. W. White, W. Krätschmer and R. H. Donald, *Nature*, 1990, **348**, 623–624.
33 Q. Guo and F. S. Li, *Phys. Chem. Chem. Phys.*, 2014, **16**, 19074–19090.
34 C. J. Li, Q. D. Zeng, Y. H. Liu, L. J. Wan, C. Wang, C. R. Wang and C. L. Bai, *ChemPhysChem*, 2003, **4**, 857–859.
35 Y. L. Huang, W. Chen, H. Li, J. Ma, J. Pflaum and A. T. S. Wee, *Small*, 2010, **6**, 70–75.
36 L. Feng, T. Wang, Z. J. Tao, J. M. Huang, G. H. Li, Q. Xu, S. L. Tait and J. F. Zhu, *ACS Nano*, 2019, **13**, 10603–10611.
37 A. L. Pinardi, G. Biddau, K. van De Ruit, G. Otero-Irurueta, S. Gardonio, S. Lizzit, R. Schennach, C. F. J. Flipse, M. F. Lopez, J. Mendez, R. Perez and J. A. Martin-Gago, *Nanotechnology*, 2014, **25**, 385602.
38 C. D. Liu, Z. H. Qin, J. A. Chen, Q. M. Guo, Y. H. Yu and G. Y. Cao, *J. Chem. Phys.*, 2011, **134**, 044707.
39 E. Delamarche, B. Michel, H. Kang and Ch. Gerber, *Langmuir*, 1994, **10**, 4103–4108.